JVI Journals.ASM.org

Genetic Analysis of the Localization of APOBEC3F to Human Immunodeficiency Virus Type 1 Virion Cores

John P. Donahue,[a] Rebecca T. Levinson,[b] Jonathan H. Sheehan,[c] Lorraine Sutton,[a] Harry E. Taylor,[e] Jens Meiler,[d] Richard T. D'Aquila,[e] Chisu Song[e]

Division of Infectious Diseases, Department of Medicine, Vanderbilt University School of Medicine, Nashville, Tennessee, USA[a]; Center for Human Genetics Research, Vanderbilt University School of Medicine, Nashville, Tennessee, USA[b]; Center for Structural Biology and Department of Biochemistry, Vanderbilt University, Nashville, Tennessee, USA[c]; Center for Structural Biology, Institute for Chemical Biology, and Departments of Chemistry, Pharmacology, and Biomedical Informatics, Vanderbilt University, Nashville Tennessee, USA[d]; Division of Infectious Diseases and Northwestern HIV Translational Research Center, Department of Medicine, Northwestern University Feinberg School of Medicine, Chicago, Illinois, USA[e]

ABSTRACT

Members of the APOBEC3 family of cytidine deaminases vary in their proportions of a virion-incorporated enzyme that is localized to mature retrovirus cores. We reported previously that APOBEC3F (A3F) was highly localized into mature human immunodeficiency virus type 1 (HIV-1) cores and identified that L306 in the C-terminal cytidine deaminase (CD) domain contributed to its core localization (C. Song, L. Sutton, M. Johnson, R. D'Aquila, J. Donahue, J Biol Chem 287:16965–16974, 2012, http://dx.doi.org/10.1074/jbc.M111.310839). We have now determined an additional genetic determinant(s) for A3F localization to HIV-1 cores. We found that one pair of leucines in each of A3F's C-terminal and N-terminal CD domains jointly determined the degree of localization of A3F into HIV-1 virion cores. These are A3F L306/L368 (C-terminal domain) and A3F L122/L184 (N-terminal domain). Alterations to one of these specific leucine residues in either of the two A3F CD domains (A3F L368A, L122A, and L184A) decreased core localization and diminished HIV restriction without changing virion packaging. Furthermore, double mutants in these leucine residues in each of A3F's two CD domains (A3F L368A plus L184A or A3F L368A plus L122A) still were packaged into virions but completely lost core localization and anti-HIV activity. HIV virion core localization of A3F is genetically separable from its virion packaging, and anti-HIV activity requires some core localization.

IMPORTANCE

Specific leucine-leucine interactions are identified as necessary for A3F's core localization and anti-HIV activity but not for its packaging into virions. Understanding these signals may lead to novel strategies to enhance core localization that may augment effects of A3F against HIV and perhaps of other A3s against retroviruses, parvoviruses, and hepatitis B virus.

The members of the apolipoprotein B mRNA-editing enzyme catalytic, polypeptide-like (APOBEC3, or A3) family of cytidine deaminases vary in several properties, and understanding these biological differences will be critical to exploit their potential for therapeutic use in humans. A3s differentially block replication of endogenous retrotransposons (1–8), endogenous retroviruses (9–11), exogenous retroviruses (12–18), adeno-associated virus (19, 20), and hepadnavirus (21–23). Family members also differ in potency of virus restriction, deaminase target sequence specificity, relative magnitude of cytidine deaminase-dependent antiviral activity, and evasion of viral countermeasures, such as the virion infectivity factor (Vif) of human immunodeficiency virus type 1 (HIV-1).

We recently reported that A3F and A3G, two family members that are relevant for human restriction of HIV-1 replication, differed in their relative magnitude of localization to virion cores (24). This is consistent with variation across the A3 family in the proportion of virion-packaged enzyme localized to cores. Mouse APOBEC3 (mA3) was localized in the cores of mouse mammary tumor virus and murine leukemia virus. It has antiviral activity against those viruses (25–27). Increasing virion-incorporated mA3 also increased the amount localized to cores (25). It also has been reported that human APOBEC3A (A3A) was not localized to HIV-1 cores and lacked HIV-1 restriction activity despite virion incorporation; however, it gained antiviral activity when fused to another protein that promoted its localization into virion cores (28, 29).

The current work focused on further characterizing genetic determinants of the high degree of core localization of A3F (24) and studying whether the degree of A3F core localization affects retroviral restriction. In addition, we tested the hypothesis that the magnitude of A3F's localization into the mature viral core is not determined only by the amount that is packaged into the virion (24, 25). This hypothesis was suggested by several earlier results (24). Previously, we demonstrated that a chimeric A3F with its

Received 1 August 2014 **Accepted** 7 December 2014

Accepted manuscript posted online 10 December 2014

Citation Donahue JP, Levinson RT, Sheehan JH, Sutton L, Taylor HE, Meiler J, D'Aquila RT, Song C. 2015. Genetic analysis of the localization of APOBEC3F to human immunodeficiency virus type 1 virion cores. J Virol 89:2415–2424. doi:10.1128/JVI.01981-14.

Editor: S. R. Ross

Address correspondence to Richard T. D'Aquila, richard.daquila@northwestern.edu, or Chisu Song, chisu.song@northwestern.edu.

Supplemental material for this article may be found at http://dx.doi.org/10.1128/JVI.01981-14.

doi:10.1128/JVI.01981-14

N-terminal CD domain replaced by glutathione *S*-transferase (GST) maintained a level of incorporation into HIV-1 virions similar to that of the wild-type (WT) A3F but exhibited decreases in both core localization and HIV restriction (24). The data presented here identified specific amino acid residues in A3F that play crucial roles for core localization and viral restriction without changing packaging into retrovirus virions. Our results suggest that studying core localization will help efforts to increase activities of A3F and other A3s against HIV, other retroviruses, hepatitis B virus (HBV), and parvoviruses.

MATERIALS AND METHODS

Cell lines and culture conditions. HEK293T cells were obtained from the ATCC. TZM-bl cells were obtained through the NIH AIDS Research and Reference Reagent Program from John C. Kappes, Xiaoyun Wu, and Tranzyme, Inc. The TZM-bl indicator cell line, used for infectivity assays, is a genetically engineered HeLa cell clone expressing CD4, CXCR4, CCR5, and Tat-responsive firefly luciferase and *Escherichia coli* β-galactosidase under the control of an HIV-1 long terminal repeat. HEK293T and TZM-bl cells were maintained in Dulbecco's modified Eagle medium (DMEM; containing 4.5 g/liter glucose, L-glutamine, and sodium pyruvate) plus 10% fetal bovine serum, 50 IU/ml penicillin, and 50 μg/ml streptomycin at 37°C and 5% CO_2.

Plasmids. A pNL4.3 Vif-null mutant, in which tandem nonsense mutations were introduced in codons 26 and 27 of the Vif open reading frame, was constructed by Ann Sheehy and acquired with her permission from Una O'Doherty. The NL4.3 Vif-null clone originally was derived from a full-length infectious HIV-1 clone, pNL4.3, and was isogenic with it except for the nonsense mutations in the Vif gene. The A3F expression plasmid was constructed as described before (24). The pcDNA3.1 HA-A3F expression plasmid was constructed by PCR amplification of A3F sequences from pcDNA3.1 A3F using an A3F-specific forward primer encoding the hemagglutinin (HA) epitope with a 5′-XbaI site and the vector-specific bovine growth hormone (BGH) reverse primer. Amplified HA-A3F DNA fragments were digested with XbaI and HindIII and inserted in XbaI/HindIII-digested pcDNA3.1(−). The resulting construct was confirmed by DNA sequencing. The A3C expression plasmid was obtained through the NIH AIDS Research and Reference Reagent Program, Division of AIDS, NIAID, NIH, deposited by B. M. Peterlin and Y.-H. Zheng (30). The pcDNA3.1 HA-A3F/C-Tail expression plasmid, in which A3F C-terminal amino acid residues 348 to 373 were replaced with A3C C-terminal residues 165 to 190, was constructed by ligating the C-terminal 488-bp A3C XbaI/BsrGI fragment with the N-terminal 1,064-bp XbaI/BsrGI fragment from pcDNA-HA-A3F in pcDNA3.1(−). Mutations were introduced into the pcDNA-HA-A3F plasmid template using appropriate mutagenic primers by a mega-primer PCR method as described previously (31). Mutations were confirmed by DNA sequencing. The sequences of primers used for the construction of all expression plasmids are available upon request.

Antibodies. The following antibody was obtained through the NIH AIDS Research and Reference Reagent Program, Division of AIDS, NIAID, NIH: anti-APOBEC3F(C18) polyclonal antibody, which recognizes the C-terminal tail of A3F, from M. Malim (32). Glyceraldehyde-3-phosphate dehydrogenase (GAPDH) and anti-β-actin monoclonal antibody (clone AC-74) were from Sigma. Anti-HA rabbit polyclonal antibody was from United States Biologicals. Anti-p24 monoclonal antibody 183-H12–5C was from the Vanderbilt-Meharry Center for AIDS Research Virology Core.

Immunoblotting. HEK293T cells were plated at a density of 6×10^5 cells/well in a 6-well culture plate 24 h prior to transfection with 1 μg of pNL4.3 Vif-null and various amounts of HA-A3F WT, HA-A3F/C-Tail, or other A3F mutants, as indicated in individual figure legends. Linear polyethylenimine (PEI; 25 kDa; Polysciences, Inc.) was used as described previously (33). Forty-eight hours after transfection, cells were lysed in 250 μl of cell lysis buffer (1× Dulbecco's phosphate-buffered saline [Mediatech, Inc.], 1 mM Na_2EDTA, 0.5% [vol/vol] Triton X-100, and complete mini protease inhibitor mixture without Na_2EDTA [Roche]) and centrifuged at 10,000 × *g* for 5 min at 4°C. Cell lysates were combined with 25 μl of 2× SDS-protein sample buffer (100 mM Tris-HCl, pH 6.8, 4 mM Na_2EDTA, 4% SDS, 4% 2-mercaptoethanol, 20% glycerol, 0.1% bromphenol blue), heated at 100°C for 5 min, and analyzed by electrophoresis through a 12.5% SDS-polyacrylamide gel. After electrophoresis, separated proteins were transferred to an Immobilon-P membrane (Millipore) and processed for Western blot analysis using protein-specific antibodies with chemiluminescent detection. Control experiments also evaluated if A3F-transfected HEK293T cells secrete microvesicles containing A3F, and no evidence of this was identified. Six million 293T cells were transiently transfected with 12 μg of A3F expression plasmids, either the WT or mutants (A3F L122A, L184A, and L368A). Cell lysates and supernatant fluids were collected 2 days after transfection. Supernatant fluids were processed exactly as were those containing viral particles for sucrose density gradient analyses (described below). The resulting cell lysates and centrifuged supernatant fluids were analyzed using immunoblotting, with blotting for GAPDH in cell lysates as a positive control. No A3F immunoreactivity was detectable in the centrifuged supernatants, despite abundant cellular expression of each A3F and GAPDH (data not shown). This is consistent with a lack of microvesicle secretion from HEK293T cells, as previously reported by others (34).

Sucrose density gradient centrifugation. HEK293T cells were plated at a density of 6×10^6 cells/100-mm culture dish 24 h prior to transfection. Cells were cotransfected with 15 μg of pNL4.3 Vif-null proviral clone and various amounts of A3 expression plasmid DNA, as indicated in the individual figure legends. Culture supernatants were collected 48 h after transfection, and cellular debris was removed by centrifugation or filtration through a 0.45-μm filter. HIV-1 particles then were concentrated by ultracentrifugation (100,000 × *g* for 3 h at 4°C) through a 20% (wt/vol) sucrose cushion in STE buffer (10 mM Tris-HCl, pH 7.4, 100 mM NaCl, 1 mM EDTA). Pelleted virions were resuspended in 300 μl of STE buffer and subjected to ultracentrifugation (130,000 × *g* for 16 h at 4°C) through a layer of 1% Triton X-100 into a linear 30 to 70% (wt/vol) sucrose density gradient, as described previously (35). After centrifugation, 1-ml fractions were collected from the top of the gradient and stored at −20°C. Specific proteins in individual fractions were analyzed by SDS-PAGE and immunoblotting. A 0.1-ml volume of each fraction was diluted with 0.1 ml STE buffer, and the protein was precipitated with an equal volume of 20% trichloroacetic acid on ice for 30 min. The protein precipitate was washed twice with 0.3 ml acetone, air dried, and dissolved in 25 μl of 2× SDS-protein sample buffer. Samples were heated at 100°C for 5 min, and 5 μl of each was fractionated by electrophoresis through a 12.5% SDS-polyacrylamide gel. After electrophoresis, separated proteins were transferred to an Immobilon-P membrane and processed for Western blot analysis using protein-specific antibodies with chemiluminescent detection.

Viral infectivity assay. TZM-bl indicator cells were plated at a density of 10,000 cells/well in a 96-well culture plate 24 h prior to infection and incubated at 37°C (5% CO_2). On the day of infection, the culture medium was removed and the cells inoculated in triplicate with 100 μl of 2-fold serial dilutions of viral supernatants in culture medium containing 20 μg/ml DEAE-dextran. After 24 h of incubation, culture medium was removed from each well and replaced with 100 μl of britelite plus luciferase assay substrate (PerkinElmer). Following 5 min of incubation at room temperature, 75 μl of each cell lysate was transferred to a 96-well OptiPlate 96 (PerkinElmer), and luminescence was measured in a VICTOR X2 multilabel reader (PerkinElmer).

Generation of A3F structural model. An A3F model was built using Rosetta 3.3, a software suite for predicting and designing protein structures, protein folding mechanisms, and protein-protein interactions (36). The 1.38-Å-resolution structure of A3G, Protein Data Bank (PDB) entry 3V4K (37), was used to build this model in order to gain more information about amino acid side chains than is present in the published structure of a modified A3F C-terminal CD domain, PDB entry 4IOU (38). The

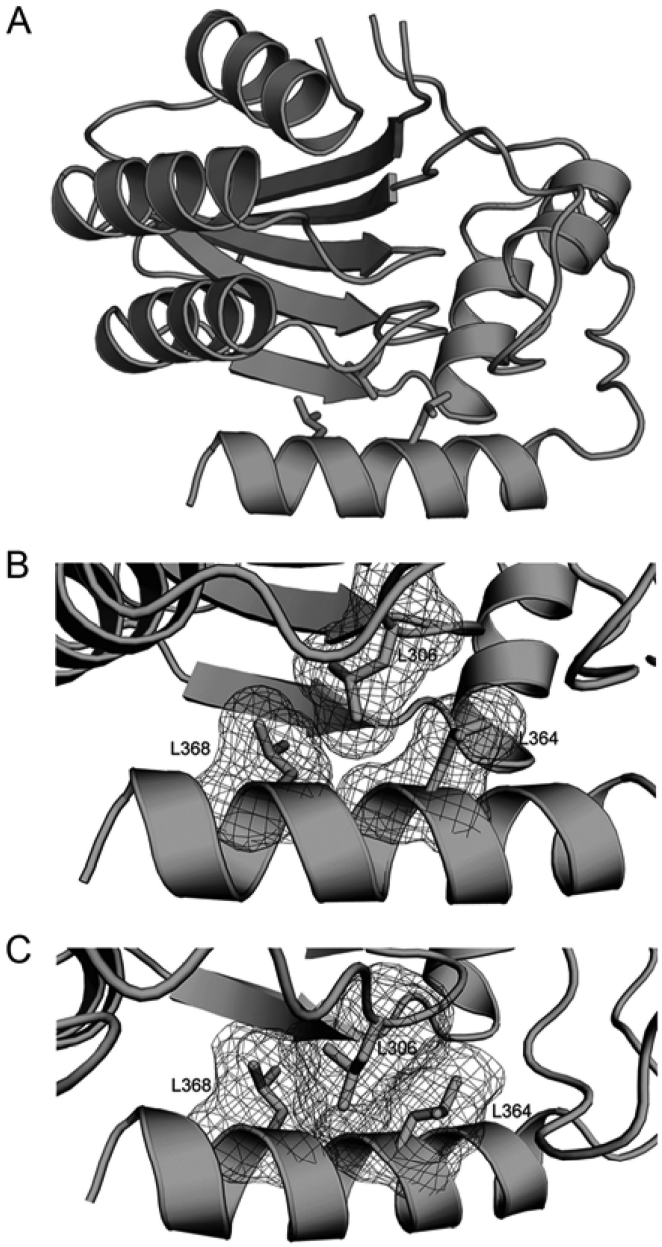

FIG 1 A3F structural models are consistent with L306 interacting with L368. (A) The structure of the entire modified A3F C-terminal CD domain (PDB entry 4IOU) (38), resolved to 2.75 Å, is depicted. (B) The relevant C-terminal region is magnified from the published determination of the structure of the A3F C-terminal CD domain (PDB entry 4IOU) (38). The α-helix 6 is on the bottom, with the C terminus of the protein to the left. The DNA substrate recognition loop between β-sheet 4 and α-helix 4 is on the top and includes L306, which is oriented downwards. L368 in α-helix 6 is to the left of L306 and oriented upward. L364 in α-helix 6 is to the right of L306 and oriented upward. L306 is closer to L368 than L364. The amino acid side chains are not fully built in this model, as deposited in the PDB. The wire mesh-like overlay is a representation of the volume of the amino acid side chains in the model. (C) The same potential interaction was seen in different models of A3F based on homology to the better-resolved (1.38 Å) structure of a modified A3G C-terminal CD domain (PDB entry 3V4K) (37). One representative homology model of A3F from among the best-scoring models (using Rosetta 3.3) (36) is depicted. The wire mesh-like overlay is a representation of the volume of the amino acid side chains in the model. α-Helix 6 is on the bottom, with the C terminus of the protein to the left. The DNA substrate recognition loop between β-sheet 4 and α-helix 4 is at the top of the figure and includes L306, which is oriented downwards. L368 in α-helix 6 is to the left of L306 and oriented upward. L364 in α-helix 6 is to the right of L306 and oriented upward. Distances are less than 4 Å and are estimated to allow hydrophobic interactions between the hydrogen atoms of L306 and L368; distances are slightly greater between atoms of L306 and L364. L372 is not shown, as it is one residue before the C terminus and too distant to potentially interact with L306. There were 18 additional amino acids at the N terminus of the A3F sequence whose structure was experimentally determined (38) relative to the A3F sequence used for building models based on homology to the A3G used here. Among the residues in common between A3F used here and that described in reference 38, 93.9% of the amino acids were identical. There were differences, however, in three of the nine amino acids in the DNA substrate recognition loop from residues 307 to 315 (the loop between β-strand 4 and α-helix 4). The published crystal structures of A3G (37) and A3F (38) also differed markedly in number, sequence, and orientation of the amino acid backbone of the DNA substrate recognition loop from residues 307 to 315, although L306 was positioned very similarly in the published crystal structures of A3G (37) and A3F (38). The amino acid backbone structure of the A3F homology model determined here differed from that of PDB entry 4IOU by an overall RMSD of 3.2 Å, with a smaller difference between them specifically in α-helix 6 (RMSD of 1.5 Å), validating the homology-based model.

sequence of the C-terminal domain of A3F used for building the model (GenBank accession number NP_660341.2, residues 193 to 373) differed from that of the expression construct used in the biological experiments by a single amino acid, with the expression construct containing an isoleucine and the computational model a valine residue at amino acid 231. This difference was inadvertently introduced during cloning of the expression construct. This A3F sequence was aligned to an edited sequence of the A chain of 3V4K from which irrelevant atoms, such as ions and ligands, had been removed. This sequence alignment was used to thread the A3F sequence onto the A3G crystal structure. In a two-step procedure, loop regions missing from the 3V4K structure were constructed, the A3F model was relaxed, and A3F loops then were rebuilt to sample a larger conformational space (36, 37, 39). Twenty thousand candidate models were generated initially. The top 2,000 scoring models were clustered by root-mean-square distance (RMSD) and ranked by Rosetta energy score. The data and protocol used for Rosetta are detailed in Fig. S1 in the supplemental material. The best-scoring models of the 10 largest clusters were selected to represent the potential conformational diversity of the loops in A3F. All models were visualized and figures were made using molecular visualization software (PyMOL Molecular Graphics System, version 1.5.0.4; Schrödinger, LLC).

RESULTS

Structural model of C-terminal CD domain of A3F indicated possible hydrophobic interaction(s) between L306 and residues in α-helix 6 of the protein. In a high-resolution crystal structure of a modified A3F C-terminal CD domain, PDB entry 4IOU (38), the L306 side chain (Fig. 1A) previously identified as necessary, but not sufficient, for extensive localization of A3F into the mature virion core (24) was close to the C-terminal α-helix 6 leucines at positions 364 and 368 (Fig. 1A). These leucines, as well as L372, in the A3F C-terminal α-helix 6 each had their side chains oriented toward the interior of the protein (38). However, amino acid side chains were not fully built in the published model of the A3F structure. Therefore, structural models of A3F also were built based on homology to the highest-resolution structure of a modified A3G C-terminal CD domain published to date, which did have side chains (PDB entry 3V4K [37]), using Rosetta 3.3 (36). A model built on homology to A3G compared well to the A3F crystal structure (38) and also supported the hypothesis that L364 and L368 have hydrophobic interactions with L306. In each of the energy-minimized models of A3F structures derived from the

A3G structure (one representative structure of the top-scoring models is shown in Fig. 1B), the carbon atoms of L306 and L368 were approximately 4 Å apart or less, a distance that could permit hydrophobic interactions between L306 and L368 residues. The distances estimated between L306 and L364 were slightly greater in our models. L372 was even more distant from L306 in both the published A3F structure and the homology model based on the A3G structure, suggesting that L372 lacked the potential to interact with L306.

Deletions of the α-helix 6 residues decrease core localization of A3F. The amino acid sequence of the C-terminal α-helix 6 starts at residue 358 in A3F (38, 40–42). By introducing a stop codon in A3F at either amino acid 350 (HA-A3F 350) or 360 (HA-A3F 360), truncated mutants lacking all of the α-helix 6 region of A3F were constructed (Fig. 2A). The effect of each truncation mutant on viral core localization then was tested by cotransfecting HEK293 cells with the Vif-null NL4.3 proviral clone and the truncation mutant A3F expression plasmids. The resulting viral particles were concentrated and analyzed using sucrose density gradients followed by immunoblotting (Fig. 2B). Wild-type (WT) A3F protein concentrated in gradient fractions corresponding to mature cores (fractions 9 and 10) (Fig. 2B HA-A3F WT). However, virion HA-A3F 350 and HA-A3F 360 proteins were distributed across sucrose density gradient fractions more broadly than HA-A3F WT (Fig. 2B, second and third gradients). The majority of both truncated mutant A3F proteins were found in fractions 5 to 8, with a small amount in one core component-containing fraction.

The C-terminal α-helix 6 truncations altered more than the conserved leucines. We assessed whether residues other than the C-terminal α-helix 6 leucines (at A3F residues 364, 368, and 372) affected core localization by using a chimeric A3F-A3C mutant protein. The number of amino acid residues in the C-terminal α-helix 6 of A3C is identical to that of A3F. However, only three of these amino acids are conserved between A3C and A3F; these are the leucines corresponding to A3F L364, L368, and L372 (Fig. 2A). Using a unique restriction site, we constructed a chimera with the A3F residues starting at amino acid 348 replaced by the corresponding C-terminal 26 residues of A3C (HA-A3F/C-Tail); the A3C residues differ in every position other than the three leucines from the corresponding A3F residues (Fig. 2A, boxed region, and C). Levels of cellular expression and viral incorporation of HA-A3F/C-Tail protein were equivalent to that of HA-A3F WT (data not shown). A sucrose density gradient indicated that HA-A3F/C-Tail localized in mature virion cores as well as HA-A3F WT (Fig. 2D). HA-A3F/C-Tail also retained the same magnitude of antiviral activity against Vif-null HIV-1 NL4.3 as wild-type A3F (data not shown). These results are consistent with a role in core localization for one or more of the leucine residues in α-helix 6 of both A3C and A3F.

Mutation of L368 in the A3F C-terminal α-helix 6 diminishes A3F's core localization and its antiviral activity. Since the results described above suggested that one or more of the 3 conserved residues in the A3F C-terminal α-helix 6 (A3F L364, L368, and L372; starred in Fig. 2A) contribute to A3F's core localization, we introduced both single- and double-alanine substitution mutations into each of them (Fig. 3A). The effects of these mutations on cellular expression, viral incorporation, infectivity, and core localization of A3F were tested as described in Materials and Methods.

Levels of cellular expression (Fig. 3B) and virion incorporation (Fig. 3C) of each of the mutants with alanine replacing one of the

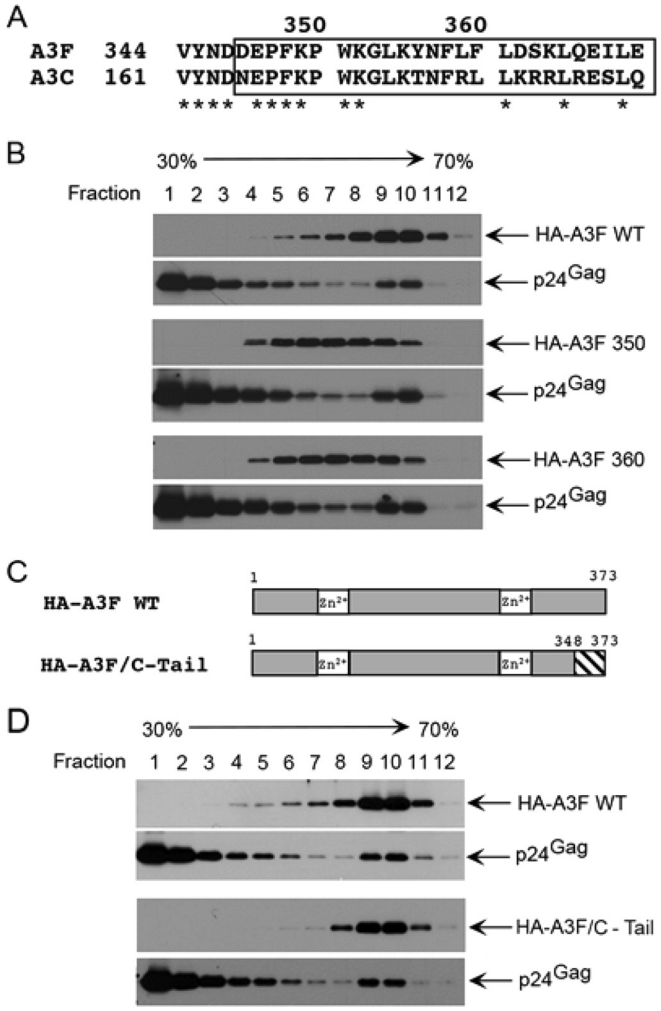

FIG 2 Truncation mutations in C-terminal domain of A3F decrease core localization of A3F, while A3F/A3C C-terminal chimeras maintain core localization, suggesting that conserved α-helix 6 leucine residues play a role in mature core localization of A3F. In these experiments, 10 μg of pNL4.3 Vif-null proviral clone and/or 3 μg of each mutant A3F expression DNA was used for transient transfection. After 2 days posttransfection, cell lysates and viral supernatants were collected to test their effect on core localization of the mutant A3Fs. (A) Sequence alignment of the C-terminal α-helix 6 of C-terminal residues of A3F and A3C. Only 3 leucines are conserved between A3F and A3C (starred) in α-helix 6, starting at amino acid 358 of A3F. DNA encoding the boxed residues of A3C (amino acids 165 to 190) replaced the boxed residues of A3F-C (amino acids 348 to 373) in the HA-A3F/C-Tail construct. Residues 350 and 360 also are depicted where the termination of A3F truncation mutants were engineered (HA-A3F 350 and HA-A3F 360, respectively). (B) Sucrose density gradient centrifugation, followed by immunoblotting using specific antibodies and chemiluminescent detection comparing mutants to HA-A3F WT (top gradient). HA-A3F 350 (second gradient) and HA-A3F 360 (third gradient) lost quantitative encapsidation. (C) Schematic representations of wild-type A3F and A3F/A3C chimeric fusion protein (HA-A3F/C-Tail) show relative locations of zinc-binding cytidine deaminase active-site motifs in white and other A3F coding sequences in gray. Hatches indicate A3C residues (A3C amino acids 165 to 190) in C-terminal α-helix 6 that replaced the A3F residues 348 to 373 in HA-A3F/C-Tail. (D) HA-A3F/C-Tail (second gradient) had mature core localization similar to that of HA-A3F-WT (first gradient), with much of the A3 being found in fractions 9 and 10 that also contain mature core-localized capsid ($p24^{Gag}$).

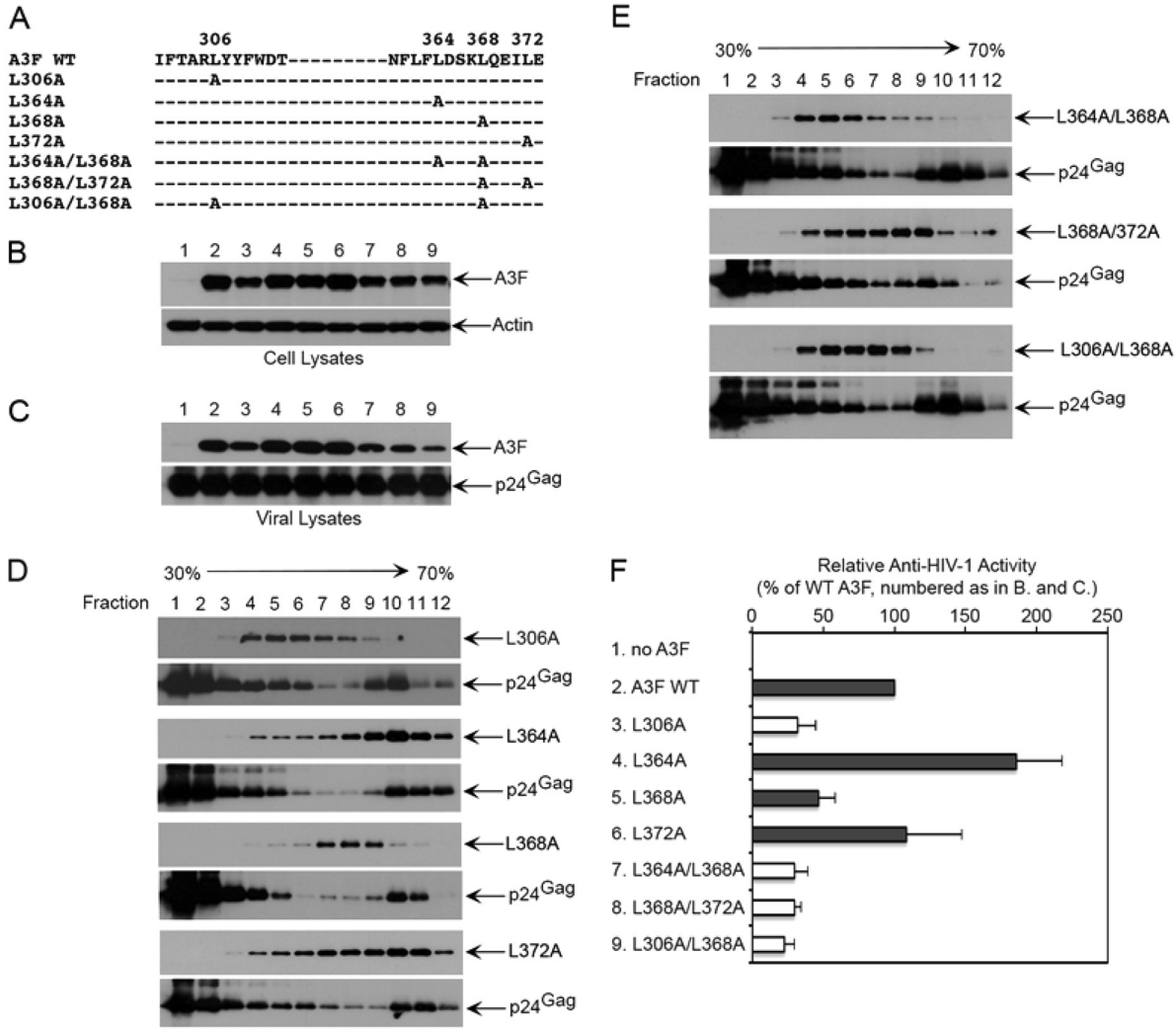

FIG 3 Mutagenesis confirms that interaction between A3F L368 and L306 is critical for quantitative encapsidation of A3F. In these experiments, 10 μg of pNL4.3 Vif-null proviral clone and 1 μg of wild-type A3F expression DNA or 3 μg of each mutant A3F expression DNA was used for transient transfection. After 2 days posttransfection, cell lysates and viral supernatants were collected to test their effect on cellular expression, viral incorporation, infectivity, and core localization of the mutant A3Fs. (A) Alanine scanning mutations introduced into conserved leucines of A3F are diagrammed. (B) Immunoblotting of cell lysates shows cellular expression of HA-tagged A3F variants relative to that of the actin loading control. Expression is decreased for L306A and each double mutant relative to that of HA-A3F-WT and the single α-helix 6 mutants (L364A, L368A, and L372A). (C) Immunoblotting of virion lysates shows virion incorporation of HA-tagged A3F variants relative to that of HIV $p24^{Gag}$. Virion incorporation is decreased for L306A and each double mutant relative to that of HA-A3F-WT and the single α-helix 6 mutants (L364A, L368A, and L372A). (D) Sucrose density gradient centrifugation followed by immunoblotting using specific antibodies and chemiluminescent detection showed differences in quantitative encapsidation of the single mutants. L306A (top gradient) and L368A (third gradient) were not quantitatively encapsidated, whereas L364A (second gradient) and L372A (fourth gradient) were. Each gradient also shows capsid ($p24^{Gag}$) in mature core component-containing fractions. (E) Sucrose density gradient centrifugation followed by immunoblotting using specific antibodies and chemiluminescent detection showed that none of the double mutants, L306A/L368A (top gradient), L364/L368A (second gradient), and L368A/L372A (third gradient), was quantitatively encapsidated. Each gradient also shows capsid ($p24^{Gag}$) in mature core component-containing fractions. (F) Equal amounts of viral particles were used to infect TZM-bl cells to test its effect on anti-HIV-1 activity. Decreased core localization diminished restriction of Vif-null HIV-1 NL4-3 by A3F. Wild-type A3F and mutants with wild-type levels of cellular expression (Fig. 5B) and virion incorporation (Fig. 5C) are depicted as gray bars. Antiviral activity against Vif-null HIV-1 was decreased for A3F L368A (lane 5) relative to that of wild-type A3F (lane 2). L364A and L372A had activity similar to that of the wild type (lanes 4 and 6, respectively). Since decreased virion incorporation is expected to diminish restriction, variants with decreased cellular expression (Fig. 5B) and virion incorporation (Fig. 5C) were compared only to each other and are shown as white bars. Among the variants with similarly reduced virion incorporation (Fig. 5C), L306/L368 (lane 9) had anti-*Vif*-null HIV activity similar to that of the other two double mutants (lanes 7 and 8) and L306A (lane 3).

α-helix 6 conserved leucine single mutants (L364A, L368A, and L372A; Fig. 3B and C, lanes 4, 5, and 6, respectively) were comparable to those of wild-type A3F (lane 2). The single L306A mutant that was characterized previously (lane 3) had slightly lower levels of cellular protein and viral incorporation, as seen before (24). In addition, each of the double C-terminal leucine mutants (L364A/L368A, L368A/L372A, and L306A/L368A; Fig. 3C, lanes 7, 8, and 9, respectively) also had a slight decrease in levels of cellular protein (Fig. 3B) and virion incorporation (Fig. 3B and C). Of note, decreased cellular levels and virion incorporation previously were

shown not to alter the distinctive magnitude of core localization of wild-type A3F versus A3G in sucrose density gradients (see Fig. 1 and 2 in reference 24).

A3F L368A, which had levels of cellular expression and viral incorporation comparable to those of the wild-type A3F, was found predominantly in gradient fractions 6 to 8; only a small amount was present in one of the core component-containing fractions, fraction 9 (Fig. 3D, third gradient). This was similar to the lesser core localization of the A3F L306A mutant (Fig. 3D, top gradient; also see Fig. 5B in reference 24). In contrast, A3F mutants with either an L364A or L372A substitution displayed a distribution across gradient fractions similar to that of wild-type A3F; these two mutants each retained core localization similar to that of wild-type A3F (Fig. 3D, second and fourth gradients). Each of the double mutants tested that contained L368A disrupted core localization (Fig. 3E). However, both L306/L368A and L364A/L368A mutants had less protein localized to the mature core component containing fractions 9 and 10 than did the other double mutant (L368/L372) (Fig. 3E, second gradient). These results indicate that A3F L368 is one of the three α-helix 6 conserved leucines that contributes to core localization, along with A3F L306.

Comparisons of infectivity of those mutants against Vif-null HIV-1 were made across the three single α-helix 6 mutants (L364A, L368A, and L372A) that had levels of virion incorporation similar to that of wild-type A3F (Fig. 3F, gray bars), since decreased incorporation itself is expected to diminish anti-HIV restriction activity. Infectivity also was compared across the variants with similarly decreased expression and virion incorporation (L306A and each of the 3 double mutants) (Fig. 3F, white bars). HA-A3F L368A had decreased antiviral activity against Vif-null HIV-1 compared to that of HA-A3F WT (Fig. 3F, row 5). In contrast, HA-A3F L364A and HA-A3F L372A each displayed antiretroviral activity comparable to that of wild-type HA-A3F (Fig. 3F, rows 2, 4, and 6). In contrast, antiviral activity was similarly decreased among the 4 variants with decreased incorporation (Fig. 3F, white bars). Therefore, A3F L368A is the only one of these mutants that had decreased anti-HIV activity along with decreased core localization in the absence of any decrease in viral incorporation.

Homologous residues in the N-terminal domain of A3F (L122 and L184) also contribute to core localization and affect antiviral activity against Vif-null HIV-1. Amino acid sequence alignment of N- and C-terminal CD domains of A3F indicated that the C-terminal domain leucine residues critical for core localization also were conserved in the N terminus of A3F (Fig. 4A). Therefore, individual alanine substitution mutations were introduced into these homologous residues in the A3F N-terminal CD domain (L122A, L180A, L184A, and L188A) to test their effect on core localization into the HIV-1 mature virion. These were introduced through site-directed mutagenesis, and mutations were confirmed using DNA sequencing. 293T cells that were transiently transfected with the Vif-null HIV-1 NL4.3 clone and either HA-tagged WT or mutant A3Fs showed cellular expression of the single mutants (L122A, L180A, L184A, and L188A) comparable to that of wild-type A3F (Fig. 4B). Each mutant protein was incorporated into viral particles at a level similar to that of the WT (Fig. 4C). Sucrose density gradient analyses showed distributions across fractions for A3F L180A and L188A similar to that for WT A3F, with much of each mutant distributing in core component-containing fractions (Fig. 4D, second and fourth gradients). However, the majority of HA-A3F L122A and L184A were found in fractions 4 to 8, with only a small amount in one of the core component-containing fractions 9 and 10 (Fig. 4D, first and third gradients). A3F L180A and L188A had antiviral activity against Vif-null HIV-1 equivalent to that of WT A3F, while A3F L122A and L184A mutants each had reduced activity (Fig. 4E). Thus, L122A and L184A in the N-terminal domain of A3F also disrupted the extensive core localization and decreased antiviral restriction activity against Vif-null HIV-1. This corresponded to the effects of mutating the homologous C-terminal residues L306 and L368 of A3F.

Disrupting the implicated leucine pairs in both N- and C-terminal CD domains completely abrogates A3F's core localization and antiviral activity against Vif-null HIV-1. Each of the mutants studied thus far that decreased core localization (A3F L122A, L184A, L306A, and L368A) retained a single CD domain core localization signal and had a distribution in sucrose density gradient experiments similar to that of A3G (Fig. 1 and 2 in reference 24). In other words, some protein localized to core fractions, albeit less so than for WT A3F. We next tested whether mutating the two leucine pairs, one each in the N- and C-terminal CD domains of A3F, thereby affecting both domains, would more markedly affect core localization. We constructed double mutants with one leucine in each CD domain changed to alanine; the mutants were A3F L122A/L368A and L184A/L368A. (Since the cellular expression level of the L306A mutant is lower than that of WT A3F, we did not include that substitution in these double mutants.) The effects of the double mutants were tested on cellular expression, viral incorporation, antiviral activity, and core localization, as described in Materials and Methods. The double mutants displayed levels of cellular expression and viral incorporation similar to that of wild-type A3F (Fig. 5A and B). However, both A3F L122A/L368A and L184A/L368A mutants were localized completely outside mature cores (Fig. 5C) with no appreciable antiviral activity against Vif-null HIV-1 (Fig. 5D).

DISCUSSION

A pair of leucines in each A3F CD domain is identified here as being necessary for core localization: L368 together with the previously described L306 in the C-terminal CD domain and L122 with L184 in the N-terminal CD domain. This extends our previous report that a greater proportion of virion-incorporated A3F than A3G colocalized with components of the mature virion core in linear sucrose density gradients following mild detergent treatment. Subsequently, others confirmed greater core localization of A3F than A3G using imaging of fluorescent-tagged fusion proteins (43), validating results of the density gradient methodology used here with an independent experimental approach. Our earlier results also identified that A3F had two core localization signals (24). The current results add further evidence that signals in each of A3F's two CD domains work together to increase localization into the HIV-1 viral mature core. Substituting an alanine for one of the leucines in a single pair in one A3F domain decreased its core localization and restriction of Vif-null HIV-1. In contrast, substituting an alanine for a leucine in both of these leucine pairs in each domain completely abrogated A3F's core localization and restriction, even when virion incorporation itself was not affected. Further, these results indicate that core localization is genetically separable from virion packaging, as suggested by several earlier

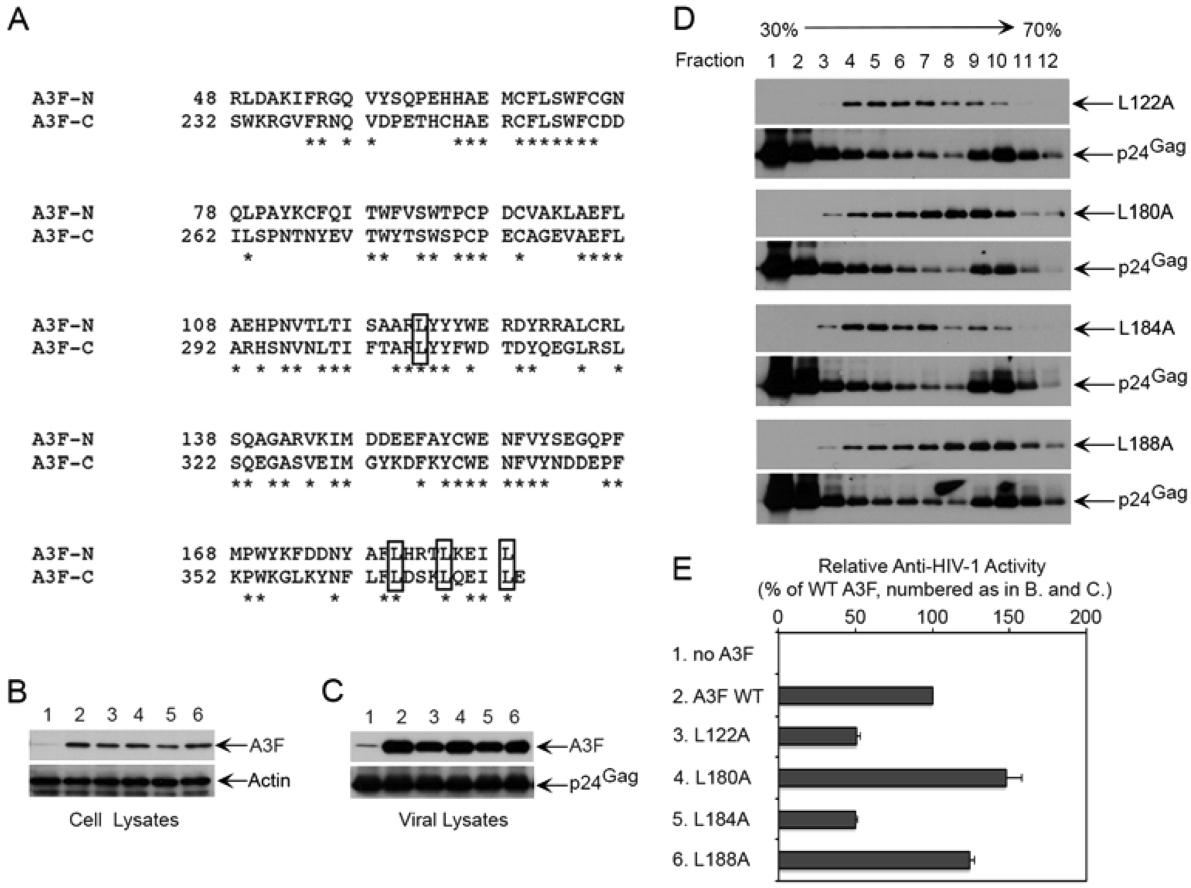

FIG 4 N-terminal leucine residues homologous to the C-terminal leucine residues also are required for A3F core localization and antiviral activity against Vif-null HIV-1. In these experiments, 10 μg of pNL4.3 Vif-null proviral clone and 1 μg of the wild type or 3 μg of each mutant A3F expression DNA was used for transient transfection. After 2 days posttransfection, cell lysates and viral supernatants were collected to test their effect on cellular expression, viral incorporation, infectivity, and core localization of the mutant A3Fs. (A) Amino acid sequence alignment of N and C termini of A3F. Leucine residues common to both N and C termini are highlighted with boxes. (B) Immunoblotting of cell lysates shows cellular expression of HA-tagged A3F variants relative to that of the actin loading control. Expression was similar for all lysates. (C) Immunoblotting of virion lysates shows virion incorporation of HA-tagged A3F variants relative to that for HIV p24^{Gag}. Virion incorporation was similar for all lysates. (D) Sucrose density gradient centrifugation and Western blotting using specific antibodies and chemiluminescent detection showed differences in core localization of the single mutants. L122A (top gradient) and L184A (third gradient) were not localized well to cores, as opposed to L180A (second gradient) and L188A (fourth gradient). Each gradient also shows capsid (p24^{Gag}) in mature core component-containing fractions. (E) Equal amounts of viral particles were used to infect TZM-bl cells to test their effect on anti-HIV-1 activity. Antiviral activity against Vif-null HIV-1 was decreased for A3F with L122A (row 3) and L184A (row 5) mutants that lost the majority of core localization relative to that of wild-type A3F (row 1). A3F L180A (row 4) and A3F L188A (row 6) had activity similar to that of wild-type A3F.

results (24, 44), and that core localization contributes to the anti-HIV activity of A3F.

Structural modeling suggested that two leucines in the C-terminal domain α-helix 6 region of A3F (L364 and L368) were in close enough proximity for hydrophobic interaction within the interior of the protein with L306, which was previously characterized as contributing to A3F core localization. A3F mutants with truncations of the C-terminal α-helix 6 did not localize to cores, consistent with a role for α-helix 6. To exclude the possibility that residues other than the leucines in α-helix 6 contributed to core localization, we studied a chimeric protein in which the C-terminal α-helix 6 of A3F was replaced with the homologous region from A3C. The leucines corresponding to A3F L364, L368, and L372 were the only residues unchanged from those in A3F in this chimeric protein. The finding that this chimera was localized to cores similarly to A3F led to mutagenesis of each of the 3 leucine residues (364, 368, and 372). A3F L368A in the C-terminal deaminase domain decreased core localization; no change was seen with the mutagenesis of either of the other two conserved leucines in α-helix 6, A3F L364A or L372A. This confirmed that L306 and L368 both were necessary for core localization.

These two leucines in the C-terminal domain, L306 and L368, of A3F are in close enough proximity for hydrophobic interaction with each other in the published A3F C-terminal domain crystal structure (38). An additional model was developed here by homology to a high-resolution structure of the A3G C-terminal domain (37, 41) in order to add more amino side chain information than was present in the solved A3F crystal structure. This also supported that A3F L368 was close enough to A3F L306 for hydrophobic or van der Waals interactions. The other A3F C-terminal α-helix 6 leucines, A3F L364 and A3F L372, were more distant from A3F L306 in both models.

The A3F C-terminal domain structure positions the L306/L368 leucine pair within the protein's interior (38). Therefore, we spec-

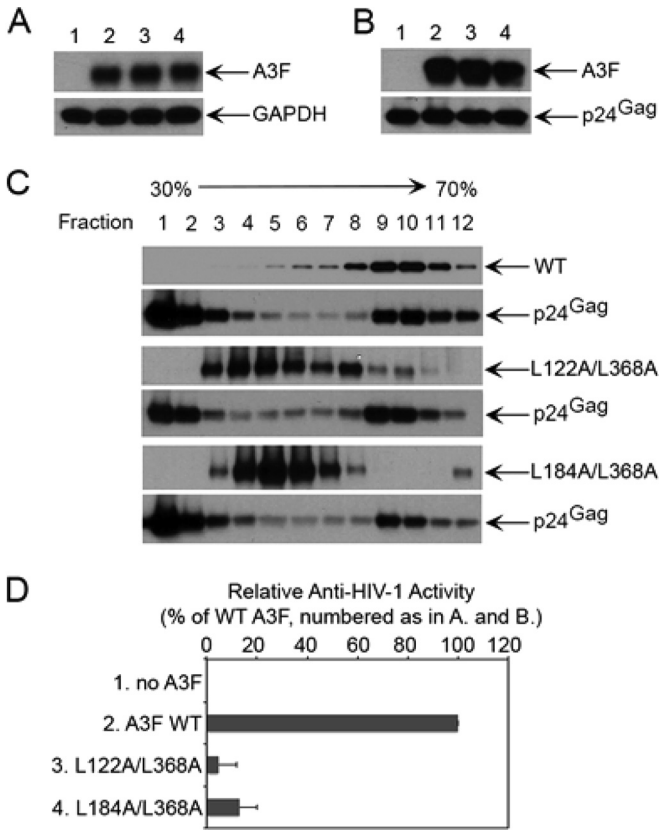

FIG 5 Double mutations into N- and C-terminal leucine residues dramatically affect core localization and anti-HIV-1 activity of A3F without affecting its viral incorporation. In these experiments, 10 μg of pNL4.3 Vif-null proviral clone and 1 μg of the wild type or 3 μg of each mutant A3F expression DNA was used for transient transfection. After 2 days posttransfection, cell lysates and viral supernatants were collected to test their effect on cellular expression, viral incorporation, infectivity, and core localization of the mutant A3Fs. (A) Immunoblot analysis shows that all of the A3Fs display similar cellular expression at the amounts used for the transfection. GAPDH was used as a loading control (lane 1, Vif-null only; lane 2, Vif-null plus WT A3F; lane 3, Vif-null plus L122/L368A A3F; lane 4, Vif-null plus L184/L368A A3F). (B) Immunoblot analysis of viral pellets shows similar levels of viral incorporation. As a loading control, p24 also was probed (lane 1, Vif-null only; lane 2, Vif-null plus WT A3F; lane 3, Vif-null plus L122/L368A A3F; and lane 4, Vif-null plus L184/L368A A3F). (C) Core localization of A3Fs was analyzed by a sucrose density gradient experiment. Unlike wild-type A3F, which was localized mainly into the core fractions, the majority of double-mutant A3Fs were found almost exclusively outside the core fractions. (D) Equal amounts of viral particles were used to infect TZM-bl cells to test their effect on anti-HIV-1 activity. Both mutant A3Fs lost almost all of their anti-HIV-1 activity compared to that of the wild-type protein.

ulate that this leucine pair, along with the homologous pair in the N-terminal domain, affect protein folding rather than mediating an interaction on the surface of the protein with a virion component that causes core localization. Indeed, the slightly decreased levels of cellular expression and virion incorporation of A3F L306A noted earlier (24) could be consistent with A3F L306A having deleterious effects on protein folding. However, none of the other three single mutations (L368A, L122A, and L184A) in the implicated leucine residues of A3F caused any decrease in levels of cellular expression or virion incorporation detected by immunoblotting. This does not completely exclude possible effects of these other mutants on protein folding. However, these results do indicate that core localization of A3F can be diminished in the absence of detectable decreases in its viral incorporation.

The determination of the mechanism whereby a leucine pair in each of two domains leads to a greater degree of virion core localization of A3F will require analyses that are beyond the scope of this report. Leucine pair-optimized folding of two domains, rather than one, may lead to twice as much interaction with a virion component that facilitates core localization. Alternatively, leucine pair-optimized folding of each domain may be needed for the correct conformation of a two-domain monomer (or oligomer) of A3F that improves a single interaction with an as-yet unidentified virion component. We hypothesize that core localization requires binding to only a subset (or one) of multiple virion components that mediate virion packaging. This may help explain why some A3 mutations affect both virion packaging and core localization while others affect only one of these processes.

It is also worth noting that earlier work showed that A3F W126A decreases localization into HIV cores in addition to impairing interaction with nucleocapsid and HIV-1 virion incorporation (24, 45). Decreased HIV virion incorporation of A3F W126A was associated with decreased binding to 7SL RNA, and no decrement of binding to HIV genomic RNA or 5S rRNA was found (45). RNase digestion of detergent-treated viral particles containing A3F (either WT, L122A, L184A, or L368A) prior to density gradient centrifugation was done as an initial test of the hypothesis that A3F core localization involves interaction with a virion RNA. However, RNase digestion did not alter the distribution of each A3F variant in the gradient (data not shown). This does not support the above-described hypothesis, although interaction with an RNA not accessible to RNase digestion cannot be excluded.

A3F mutations that specifically decreased localization to HIV cores diminished its anti-HIV restriction activity. This could be due to decreased virion core association itself or to changes in protein structure that independently affect both core association and restriction activity. Core localization of mA3 has been shown to be important for its deaminase-independent activity against Moloney murine leukemia virus and murine leukemia virus (25–27, 46) and for the anti-HIV activity of A3A (28, 29). The magnitude of loss of antiviral activity against Vif-null HIV-1 for each of the A3F mutants that had decreased core localization (A3F L122A, L184A L306A, L368A, L364A/L368A, L368A/L372A, and L306A/L368A) was similar to that of the deaminase-defective A3F E251Q, which did not have any alteration in core localization compared to wild-type A3F (data not shown). Thus, these experiments suggest that a similar diminishment in restriction activity occurs when A3F loses either its intrinsic deaminase activity or its access to the HIV genome in the core that is the target for deamination. However, intrinsic differences between different A3s (e.g., A3F versus A3G) may be more important in determining the relative antiviral potency of the different enzymes than the relative magnitude of core localization. It has been shown that A3F's deaminase activity is intrinsically limited relative to that of A3G (47), and the more core-associated A3F may not be more potent in restricting HIV than A3G (24, 32, 48).

Further study of mechanisms underlying the relatively better core localization of A3F may lead to the potential for virion engineering to therapeutically maximize antiviral effects of other A3s in the future. For example, small molecules might be developed that could stabilize a conformation that increases A3G's limited

localization into cores, which may increase its overall anti-HIV activity and decrease the potential for evasion of Vif via decreased virion incorporation (49, 50). Since the residues of A3F and A3G to which HIV-1 Vif binds in order to facilitate their proteasomal degradation are distinct from core-localizing determinants, agents being developed to antagonize Vif may not decrease core localization that enhances antiviral activity against Vif-null HIV by A3F. Since core localization is implicated in antiparvovirus activities of A3 enzymes (19, 20) and at least a portion of their anti-HBV activity (22, 51–55), increased basic understanding of core localization also holds promise for improved treatments for those viruses.

ACKNOWLEDGMENTS

We thank the NIH AIDS Reference and Reagent Program, Division of AIDS, NIAID, which provided plasmids, antibodies, and cell lines.

Grant support was provided by R01 AI29193 and T32 GM080178 from the NIH. The D'Aquila laboratory also acknowledges support from the Northwestern Medicine Catalyst Fund. Work in the Meiler laboratory is supported by the NIH (R01 GM080403, R01 MH090192, R01 GM099842, and R01 DK097376) and NSF (career 0742762).

REFERENCES

1. **Bogerd HP, Wiegand HL, Hulme AE, Garcia-Perez JL, O'Shea KS, Moran JV, Cullen BR.** 2006. Cellular inhibitors of long interspersed element 1 and Alu retrotransposition. Proc Natl Acad Sci U S A **103:**8780–8785. http://dx.doi.org/10.1073/pnas.0603313103.
2. **Chiu YL, Witkowska HE, Hall SC, Santiago M, Soros VB, Esnault C, Heidmann T, Greene WC.** 2006. High-molecular-mass APOBEC3G complexes restrict Alu retrotransposition. Proc Natl Acad Sci U S A **103:**15588–15593. http://dx.doi.org/10.1073/pnas.0604524103.
3. **Dutko JA, Schafer A, Kenny AE, Cullen BR, Curcio MJ.** 2005. Inhibition of a yeast LTR retrotransposon by human APOBEC3 cytidine deaminases. Curr Biol **15:**661–666. http://dx.doi.org/10.1016/j.cub.2005.02.051.
4. **Esnault C, Millet J, Schwartz O, Heidmann T.** 2006. Dual inhibitory effects of APOBEC family proteins on retrotransposition of mammalian endogenous retroviruses. Nucleic Acids Res **34:**1522–1531. http://dx.doi.org/10.1093/nar/gkl054.
5. **Muckenfuss H, Hamdorf M, Held U, Perkovic M, Lower J, Cichutek K, Flory E, Schumann GG, Munk C.** 2006. APOBEC3 proteins inhibit human LINE-1 retrotransposition. J Biol Chem **281:**22161–22172. http://dx.doi.org/10.1074/jbc.M601716200.
6. **Schumacher AJ, Hache G, Macduff DA, Brown WL, Harris RS.** 2008. The DNA deaminase activity of human APOBEC3G is required for Ty1, MusD, and human immunodeficiency virus type 1 restriction. J Virol **82:**2652–2660. http://dx.doi.org/10.1128/JVI.02391-07.
7. **Schumacher AJ, Nissley DV, Harris RS.** 2005. APOBEC3G hypermutates genomic DNA and inhibits Ty1 retrotransposition in yeast. Proc Natl Acad Sci U S A **102:**9854–9859. http://dx.doi.org/10.1073/pnas.0501694102.
8. **Stenglein MD, Harris RS.** 2006. APOBEC3B and APOBEC3F inhibit L1 retrotransposition by a DNA deamination-independent mechanism. J Biol Chem **281:**16837–16841. http://dx.doi.org/10.1074/jbc.M602367200.
9. **Armitage AE, Katzourakis A, de Oliveira T, Welch JJ, Belshaw R, Bishop KN, Kramer B, McMichael AJ, Rambaut A, Iversen AK.** 2008. Conserved footprints of APOBEC3G on hypermutated human immunodeficiency virus type 1 and human endogenous retrovirus HERV-K(HML2) sequences. J Virol **82:**8743–8761. http://dx.doi.org/10.1128/JVI.00584-08.
10. **Esnault C, Heidmann O, Delebecque F, Dewannieux M, Ribet D, Hance AJ, Heidmann T, Schwartz O.** 2005. APOBEC3G cytidine deaminase inhibits retrotransposition of endogenous retroviruses. Nature **433:**430–433. http://dx.doi.org/10.1038/nature03238.
11. **Lee YN, Malim MH, Bieniasz PD.** 2008. Hypermutation of an ancient human retrovirus by APOBEC3G. J Virol **82:**8762–8770. http://dx.doi.org/10.1128/JVI.00751-08.
12. **Delebecque F, Suspene R, Calattini S, Casartelli N, Saib A, Froment A, Wain-Hobson S, Gessain A, Vartanian JP, Schwartz O.** 2006. Restriction of foamy viruses by APOBEC cytidine deaminases. J Virol **80:**605–614. http://dx.doi.org/10.1128/JVI.80.2.605-614.2006.
13. **Jonsson SR, LaRue RS, Stenglein MD, Fahrenkrug SC, Andresdottir V, Harris RS.** 2007. The restriction of zoonotic PERV transmission by human APOBEC3G. PLoS One **2:**e893. http://dx.doi.org/10.1371/journal.pone.0000893.
14. **Mangeat B, Turelli P, Caron G, Friedli M, Perrin L, Trono D.** 2003. Broad antiretroviral defence by human APOBEC3G through lethal editing of nascent reverse transcripts. Nature **424:**99–103. http://dx.doi.org/10.1038/nature01709.
15. **Takeda E, Tsuji-Kawahara S, Sakamoto M, Langlois MA, Neuberger MS, Rada C, Miyazawa M.** 2008. Mouse APOBEC3 restricts friend leukemia virus infection and pathogenesis in vivo. J Virol **82:**10998–11008. http://dx.doi.org/10.1128/JVI.01311-08.
16. **Low A, Okeoma CM, Lovsin N, de las Heras M, Taylor TH, Peterlin BM, Ross SR, Fan H.** 2009. Enhanced replication and pathogenesis of Moloney murine leukemia virus in mice defective in the murine APOBEC3 gene. Virology **385:**455–463. http://dx.doi.org/10.1016/j.virol.2008.11.051.
17. **Okeoma CM, Low A, Bailis W, Fan HY, Peterlin BM, Ross SR.** 2009. Induction of APOBEC3 in vivo causes increased restriction of retrovirus infection. J Virol **83:**3486–3495. http://dx.doi.org/10.1128/JVI.02347-08.
18. **Okeoma CM, Petersen J, Ross SR.** 2009. Expression of murine APOBEC3 alleles in different mouse strains and their effect on mouse mammary tumor virus infection. J Virol **83:**3029–3038. http://dx.doi.org/10.1128/JVI.02536-08.
19. **Chen H, Lilley CE, Yu Q, Lee DV, Chou J, Narvaiza I, Landau NR, Weitzman MD.** 2006. APOBEC3A is a potent inhibitor of adeno-associated virus and retrotransposons. Curr Biol **16:**480–485. http://dx.doi.org/10.1016/j.cub.2006.01.031.
20. **Narvaiza I, Linfesty DC, Greener BN, Hakata Y, Pintel DJ, Logue E, Landau NR, Weitzman MD.** 2009. Deaminase-independent inhibition of parvoviruses by the APOBEC3A cytidine deaminase. PLoS Pathog **5:**e1000439. http://dx.doi.org/10.1371/journal.ppat.1000439.
21. **Baumert TF, Rosler C, Malim MH, von Weizsacker F.** 2007. Hepatitis B virus DNA is subject to extensive editing by the human deaminase APOBEC3C. Hepatology **46:**682–689. http://dx.doi.org/10.1002/hep.21733.
22. **Rosler C, Kock J, Kann M, Malim MH, Blum HE, Baumert TF, von Weizsacker F.** 2005. APOBEC-mediated interference with hepadnavirus production. Hepatology **42:**301–309. http://dx.doi.org/10.1002/hep.20801.
23. **Suspene R, Guetard D, Henry M, Sommer P, Wain-Hobson S, Vartanian JP.** 2005. Extensive editing of both hepatitis B virus DNA strands by APOBEC3 cytidine deaminases in vitro and in vivo. Proc Natl Acad Sci U S A **102:**8321–8326. http://dx.doi.org/10.1073/pnas.0408223102.
24. **Song C, Sutton L, Johnson M, D'Aquila R, Donahue J.** 2012. Signals in APOBEC3F N-terminal and C-terminal deaminase domains each contribute to encapsidation in HIV-1 virions and are both required for HIV-1 restriction. J Biol Chem **287:**16965–16974. http://dx.doi.org/10.1074/jbc.M111.310839.
25. **MacMillan AL, Kohli RM, Ross SR.** 2013. APOBEC3 inhibition of mouse mammary tumor virus infection: the role of cytidine deamination versus inhibition of reverse transcription. J Virol **87:**4808–4817. http://dx.doi.org/10.1128/JVI.00112-13.
26. **Rulli SJ, Jr, Mirro J, Hill SA, Lloyd P, Gorelick RJ, Coffin JM, Derse D, Rein A.** 2008. Interactions of murine APOBEC3 and human APOBEC3G with murine leukemia viruses. J Virol **82:**6566–6575. http://dx.doi.org/10.1128/JVI.01357-07.
27. **Zhang L, Li X, Ma J, Yu L, Jiang J, Cen S.** 2008. The incorporation of APOBEC3 proteins into murine leukemia viruses. Virology **378:**69–78. http://dx.doi.org/10.1016/j.virol.2008.05.006.
28. **Aguiar RS, Lovsin N, Tanuri A, Peterlin BM.** 2008. Vpr.A3A chimera inhibits HIV replication. J Biol Chem **283:**2518–2525. http://dx.doi.org/10.1074/jbc.M706436200.
29. **Goila-Gaur R, Khan M, Miyagi E, Kao S, Strebel K.** 2007. Targeting APOBEC3A to the viral nucleoprotein complex confers antiviral activity. Retrovirology **4:**61. http://dx.doi.org/10.1186/1742-4690-4-61.
30. **Zheng YH, Irwin D, Kurosu T, Tokunaga K, Sata T, Peterlin BM.** 2004. Human APOBEC3F is another host factor that blocks human immunodeficiency virus type 1 replication. J Virol **78:**6073–6076. http://dx.doi.org/10.1128/JVI.78.11.6073-6076.2004.
31. **Song C, Dubay SR, Hunter E.** 2003. A tyrosine motif in the cytoplasmic domain of Mason-Pfizer monkey virus is essential for the incorporation of glycoprotein into virions. J Virol **77:**5192–5200. http://dx.doi.org/10.1128/JVI.77.9.5192-5200.2003.
32. **Holmes RK, Koning FA, Bishop KN, Malim MH.** 2007. APOBEC3F can inhibit the accumulation of HIV-1 reverse transcription products in the

absence of hypermutation. Comparisons with APOBEC3G. J Biol Chem **282:**2587–2595. http://dx.doi.org/10.1074/jbc.M607298200.
33. **Durocher Y, Perret S, Kamen A.** 2002. High-level and high-throughput recombinant protein production by transient transfection of suspension-growing human 293-EBNA1 cells. Nucleic Acids Res **30:**E9. http://dx.doi.org/10.1093/nar/30.2.e9.
34. **Taylor HE, Khatua AK, Popik W.** 2014. The innate immune factor apolipoprotein L1 restricts HIV-1 infection. J Virol **88:**592–603. http://dx.doi.org/10.1128/JVI.02828-13.
35. **Kotov A, Zhou J, Flicker P, Aiken C.** 1999. Association of Nef with the human immunodeficiency virus type 1 core. J Virol **73:**8824–8830.
36. **Leaver-Fay A, Tyka M, Lewis SM, Lange OF, Thompson J, Jacak R, Kaufman K, Renfrew PD, Smith CA, Sheffler W, Davis IW, Cooper S, Treuille A, Mandell DJ, Richter F, Ban YE, Fleishman SJ, Corn JE, Kim DE, Lyskov S, Berrondo M, Mentzer S, Popovic Z, Havranek JJ, Karanicolas J, Das R, Meiler J, Kortemme T, Gray JJ, Kuhlman B, Baker D, Bradley P.** 2011. ROSETTA3: an object-oriented software suite for the simulation and design of macromolecules. Methods Enzymol **487:**545–574. http://dx.doi.org/10.1016/B978-0-12-381270-4.00019-6.
37. **Li M, Shandilya SM, Carpenter MA, Rathore A, Brown WL, Perkins AL, Harki DA, Solberg J, Hook DJ, Pandey KK, Parniak MA, Johnson JR, Krogan NJ, Somasundaran M, Ali A, Schiffer CA, Harris RS.** 2012. First-in-class small molecule inhibitors of the single-strand DNA cytosine deaminase APOBEC3G. ACS Chem Biol **7:**506–517. http://dx.doi.org/10.1021/cb200440y.
38. **Bohn M-F, Shandilya S, Albin J, Kouno T, Anderson B, McDougle R, Carpenter M, Rathore A, Evans L, Davis A, Zhang J, Lu Y, Somasundaran M, Matsuo H, Harris R, Schiffer C.** 2013. Crystal structure of the DNA cytosine deaminase APOBEC3F: the catalytically active and HIV-1 Vif-binding domain. Structure **21:**1042–1050. http://dx.doi.org/10.1016/j.str.2013.04.010.
39. **Combs SA, Deluca SL, Deluca SH, Lemmon GH, Nannemann DP, Nguyen ED, Willis JR, Sheehan JH, Meiler J.** 2013. Small-molecule ligand docking into comparative models with Rosetta. Nat Protoc **8:**1277–1298. http://dx.doi.org/10.1038/nprot.2013.074.
40. **Shandilya SM, Nalam MN, Nalivaika EA, Gross PJ, Valesano JC, Shindo K, Li M, Munson M, Royer WE, Harjes E, Kono T, Matsuo H, Harris RS, Somasundaran M, Schiffer CA.** 2010. Crystal structure of the APOBEC3G catalytic domain reveals potential oligomerization interfaces. Structure **18:**28–38. http://dx.doi.org/10.1016/j.str.2009.10.016.
41. **Shlyakhtenko L, Lushnikov A, Miyagi A, Li M, Harris R, Lyubchenko Y.** 2012. Nanoscale structure and dynamics of ABOBEC3G complexes with single-stranded DNA. Biochemistry **51:**6432–6440. http://dx.doi.org/10.1021/bi300733d.
42. **Chen KM, Harjes E, Gross PJ, Fahmy A, Lu Y, Shindo K, Harris RS, Matsuo H.** 2008. Structure of the DNA deaminase domain of the HIV-1 restriction factor APOBEC3G. Nature **452:**116–119. http://dx.doi.org/10.1038/nature06638.
43. **Burdick RC, Hu WS, Pathak VK.** 2013. Nuclear import of APOBEC3F-labeled HIV-1 preintegration complexes. Proc Natl Acad Sci U S A **110:**E4780–E4789. http://dx.doi.org/10.1073/pnas.1315996110.
44. **Hache G, Liddament MT, Harris RS.** 2005. The retroviral hypermutation specificity of APOBEC3F and APOBEC3G is governed by the C-terminal DNA cytosine deaminase domain. J Biol Chem **280:**10920–10924. http://dx.doi.org/10.1074/jbc.M500382200.
45. **Wang T, Tian C, Zhang W, Sarkis PT, Yu XF.** 2008. Interaction with 7SL RNA but not with HIV-1 genomic RNA or P bodies is required for APOBEC3F virion packaging. J Mol Biol **375:**1098–1112. http://dx.doi.org/10.1016/j.jmb.2007.11.017.
46. **Sanchez-Martinez S, Aloia AL, Harvin D, Mirro J, Gorelick RJ, Jern P, Coffin JM, Rein A.** 2012. Studies on the restriction of murine leukemia viruses by mouse APOBEC3. PLoS One **7:**e38190. http://dx.doi.org/10.1371/journal.pone.0038190.
47. **Ara A, Love RP, Chelico L.** 2014. Different mutagenic potential of HIV-1 restriction factors APOBEC3G and APOBEC3F is determined by distinct single-stranded DNA scanning mechanisms. PLoS Pathog **10:**e1004024. http://dx.doi.org/10.1371/journal.ppat.1004024.
48. **Zennou V, Bieniasz PD.** 2006. Comparative analysis of the antiretroviral activity of APOBEC3G and APOBEC3F from primates. Virology **349:**31–40. http://dx.doi.org/10.1016/j.virol.2005.12.035.
49. **Haché G, Shindo K, Albin J, Harris R.** 2008. Evolution of HIV-1 isolates that use a novel Vif-independent mechanism to resist restriction by human APOBEC3G. Curr Biol **18:**819–824. http://dx.doi.org/10.1016/j.cub.2008.04.073.
50. **Hache G, Abbink TE, Berkhout B, Harris RS.** 2009. Optimal translation initiation enables Vif-deficient human immunodeficiency virus type 1 to escape restriction by APOBEC3G. J Virol **83:**5956–5960. http://dx.doi.org/10.1128/JVI.00045-09.
51. **Nguyen DH, Gummuluru S, Hu J.** 2007. Deamination-independent inhibition of hepatitis B virus reverse transcription by APOBEC3G. J Virol **81:**4465–4472. http://dx.doi.org/10.1128/JVI.02510-06.
52. **Li D, Liu J, Kang F, Guan W, Gao X, Wang Y, Sun D.** 2011. Core-APOBEC3C chimerical protein inhibits hepatitis B virus replication. J Biochem **150:**371–374. http://dx.doi.org/10.1093/jb/mvr086.
53. **Turelli P, Mangeat B, Jost S, Vianin S, Trono D.** 2004. Inhibition of hepatitis B virus replication by APOBEC3G. Science **303:**1829. http://dx.doi.org/10.1126/science.1092066.
54. **Rosler C, Kock J, Malim MH, Blum HE, von Weizsacker F.** 2004. Comment on "Inhibition of hepatitis B virus replication by APOBEC3G." Science **305:**1403. (Reply.) http://dx.doi.org/10.1126/science.1100464.
55. **Noguchi C, Hiraga N, Mori N, Tsuge M, Imamura M, Takahashi S, Fujimoto Y, Ochi H, Abe H, Maekawa T, Yatsuji H, Shirakawa K, Takaori-Kondo A, Chayama K.** 2007. Dual effect of APOBEC3G on hepatitis B virus. J Gen Virol **88:**432–440. http://dx.doi.org/10.1099/vir.0.82319-0.